Applied Catalysis B: Environmental 189 (2016) 219–225

Contents lists available at ScienceDirect

Applied Catalysis B: Environmental

journal homepage: www.elsevier.com/locate/apcatb

Stability of platinum nanoparticles supported on surface-treated carbon black

Yuki Kameya [a,*], Takuhiro Hayashi [b], Masahiro Motosuke [b,c]

[a] Department of Mechanical and Control Engineering, Tokyo Institute of Technology, Tokyo, Japan
[b] Department of Mechanical Engineering, Tokyo University of Science, Tokyo, Japan
[c] Research Institute for Science & Technology, Tokyo University of Science, Tokyo, Japan

ARTICLE INFO

Article history:
Received 14 December 2015
Received in revised form 20 January 2016
Accepted 24 February 2016
Available online 27 February 2016

Keywords:
Platinum nanoparticle
Fuel cell catalyst support
Carbon black
Surface nanostructure
in situ TEM

ABSTRACT

Platinum nanoparticles supported on carbon black (CB) are used as electrocatalysts in polymer electrolyte fuel cells, and their stability is important for the durability of the catalyst system. Here, we investigated the stability of Pt nanoparticles supported on surface-treated CB with a thermochemically developed surface nanostructure. The protruding structure of surface-treated CB was able to support Pt nanoparticles synthesized via the sodium tetrahydroborate ($NaBH_4$) reduction of hexachloroplatinic(IV) acid hexahydrate ($H_2PtCl_6{\cdot}6H_2O$) with polyvinylpyrrolidone (PVP). The dependence of Pt stability on the deposition locations on the CB surface was examined using in situ transmission electron microscope observations during heating up to 800°C. We found that the protruding parts on the CB surface function as local sites for stably supporting Pt nanoparticles. Hence, we suggest that the stability of the Pt nanoparticles can be improved using the CB surface nanostructure.

1. Introduction

Platinum nanoparticles behave as electrocatalysts in polymer electrolyte fuel cells (PEFCs), and carbon black (CB) is widely used to support them [1]. A typical PEFC catalyst layer consists of Pt nanoparticles of diameter less than 5 nm dispersed on the CB support, and catalyst degradation occurs during the PEFC operation owing to the sintering of Pt nanoparticles and oxidation of the CB support [2]. Even though many approaches have been proposed to enhance the durability of the Pt catalyst system [1,3], further improvements are needed for both catalyst particles and support materials.

CB is a carbonaceous particulate material produced by partial combustion or thermal decomposition of hydrocarbons [4]. Nascent particles are thought to form from molecular precursors such as polycyclic aromatic hydrocarbons. Because of its formation mechanism, the primary particles are nearly spherical. Several primary particles coalesce into an aggregate which is the basic morphological unit of CB. Depending on the intended applications, the physical and chemical characteristics of CB are modified by controlling the size, aggregate structure, internal crystalline structure, and surface chemistry. In a PEFC catalyst system, CB is employed as a catalyst support because of its good electrical conductivity, high surface area, and low cost [1]. In addition to these favorable characteristics, it would be more beneficial if we could add more functions to CB to enhance the stability of the supported Pt nanoparticles.

The authors investigated the kinetics of the methane and alcohol thermal decomposition under the environment where CB existed, and found the evolving surface nanostructure of CB due to continuous deposition of carbon atoms on the CB surface [5–8]. We observed that a graphitic sheet-like structure was developed and a protruding nanostructure formed over the CB surface. We have shown that surface structure development using carbon deposition is applied for a surface treatment process to enhance the oxidation resistance of CB [8]. An earlier study [9] has also demonstrated that the physical structure of the carbon surface affects the dynamic behavior of the supported catalyst nanoparticles. Thus, we expect the nanostructure of the CB surface, which is developed on initially spherical CB, to positively affect the Pt nanoparticles behavior by stably supporting them and inhibiting sintering.

To examine the deposition state of Pt nanoparticles on the support material, transmission electron microscope (TEM) observation is a useful technique [10]. In situ observations during sample heating help us to understand the dynamic behavior of nanoparticles [9,11–16]. In particular, when the support material surface is inho-

* Corresponding author at: Department of Mechanical and Control Engineering, Tokyo Institute of Technology, 2–12-1 NE-8, Ookayama, Meguro-ku, Tokyo 152–8552, Japan. Fax: +81 3 5734 3853.
E-mail addresses: kameya.y.ab@m.titech.ac.jp, yuki.kameya.jp@gmail.com (Y. Kameya).

http://dx.doi.org/10.1016/j.apcatb.2016.02.049
0926-3373/

mogeneous, the differences in the stability characteristics of the Pt nanoparticles arising from the nature of deposition sites are of interest. In such cases, in situ TEM observations are well suited to observe nanoscale phenomena.

In the present work, the stability of Pt nanoparticles supported on surface-treated CB was investigated. The CB surface nanostructure was built as described in our previous papers [5–8]. We used two types of Pt nanoparticles with respect to dispersion state on CB surface: agglomerated and monodispersed particles. The dynamic behavior of the Pt nanoparticles during heating was examined by means of in situ TEM observation. TEM images were obtained and analyzed to study the stability characteristics depending on the deposition sites on the CB surface. In addition, the interaction of Pt and CB particles during the Pt deposition process and the effect of the dispersing agent on Pt sintering are discussed.

2. Experimental

2.1. Carbon samples

Commercial CB SB905 (Asahi Carbon, Japan) was used because of its superior homogeneity in particulate properties. The mean diameter of the primary particle is 15 nm and the specific surface area is 212 m^2/g. The sample was stored in a desiccator after receiving from the manufacturer and was used as received.

2.2. Surface treatment of CB

We treated the CB surface following the thermochemical process developed in our previous studies [5–8]. The samples were placed in a vertical quartz tube reactor heated by an electric tube furnace. The gaseous carbon source (methane or ethanol vapor) was supplied with the carrier gas into the reactor. The duration of the reaction was adjusted to control the degree of surface nanostructure development.

2.3. Platinum nanoparticle synthesis and deposition on CB

After completing the CB surface treatment, Pt nanoparticles supported on CB (Pt/CB samples) were prepared via an aqueous process. The synthesis procedure is shown in Fig. 1. For the deposition of Pt agglomerates on CB, we simply mixed a commercial Pt colloid and a CB dispersion (Fig. 1(a)). Because it is difficult to obtain nonagglomerated Pt particles with this method, we used the sodium tetrahydroborate ($NaBH_4$) reduction method to prepare monodispersed Pt particles (Fig. 1(b)) [17]. The Pt precursor, hexachloroplatinic(IV) acid hexahydrate ($H_2PtCl_6{\cdot}6H_2O$), was dissolved in water to obtain a solution of 4.0 mM. Polyvinylpyrrolidone (PVP) was used to stabilize the nanoparticles, and a 12 mM (monomer unit) water solution was added to the Pt precursor solution. Sodium tetrahydroborate ($NaBH_4$) was then added to the solution to reduce the Pt salt. CB was placed into water followed by ultrasonication; the CB suspension was then mixed with the Pt precursor solution. The mixture was vigorously stirred using a magnetic stirrer, and the Pt nanoparticles were synthesized. Subsequently, centrifugation was performed to remove the large agglomerated particles. To analyze the as-synthesized well-dispersed Pt particles, we also prepared a Pt suspension without adding CB.

The size distribution and zeta potential of the Pt nanoparticles in water were measured using an ELSZ-1000 zeta potential & particle size analyzer (Otsuka electronics, Japan). The particle size analysis was based on dynamic light scattering (DLS) scheme.

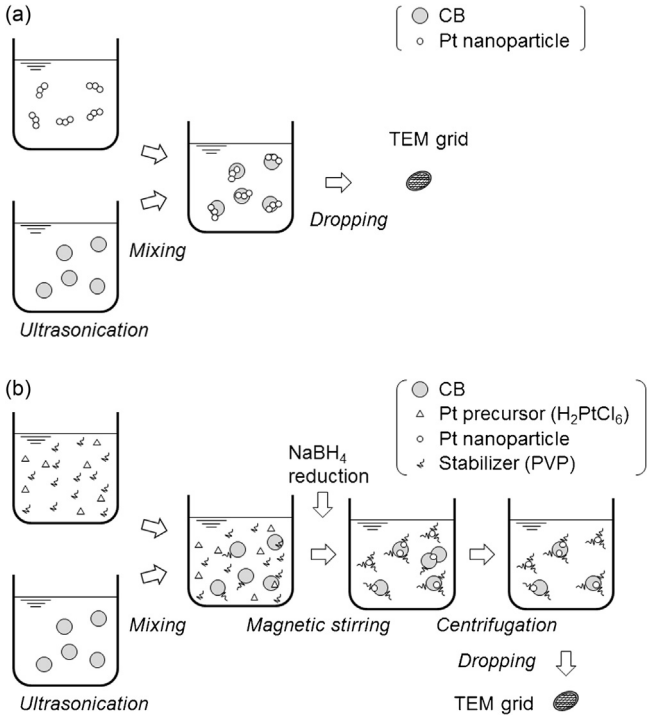

Fig. 1. Schematic illustration of the aqueous sample synthesis procedures: (a) colloid method, and (b) $NaBH_4$ reduction method.

2.4. Transmission electron microscopy

To observe the Pt/CB samples during heating, a JEM-2100F transmission electron microscope (JEOL, Japan) was used. The microscope was operated at an acceleration voltage of 200 kV. The samples were deposited on a Cu TEM grid (200 mesh) with an amorphous carbon film (U1003, EMJapan, Japan) and heated with a heating holder (Gatan model 652). The TEM images were analyzed with the ImageJ software [18].

3. Results and discussion

3.1. Dynamic behavior of agglomerated Pt nanoparticles

We used the aqueous suspension of agglomerated Pt nanoparticles to prepare samples for the first TEM heating experiment. The primary particle diameter was about 3 nm based on the TEM observations, and the number-averaged diameter evaluated by DLS was 23 nm (Fig. 2). This suggested that the Pt nanoparticles were not monodispersed but already agglomerated when in suspension. We performed TEM observations of the Pt nanoparticles deposited on CB and calculated the radius of gyration R_g from the obtained images [19,20]. The radius of gyration of the agglomerates consisting of primary particles is

$$R_g{}^2 = \frac{\sum_i (r_i - r_c)^2 m_i}{\sum_i m_i}, \quad (1)$$

where $r_i - r_c$ is the distance from the center of mass of an agglomerate to a primary particle i, and m_i is the mass of primary particle i. To apply this R_g calculation to the TEM image analysis, we used the image area of the particles instead of mass. Although this is typical in TEM image analysis [19,20], the obtained value is based on 2D data, whereas the data obtained by DLS are intrinsically 3D. The averaged $2R_g$ was about 18 nm and close to the mean diameter of 23 nm based on DLS, which means that remarkable agglomeration did not occur during deposition.

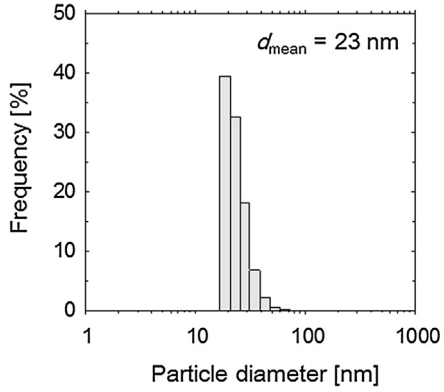

Fig. 2. Size distribution of agglomerated Pt nanoparticles in suspension measured by DLS.

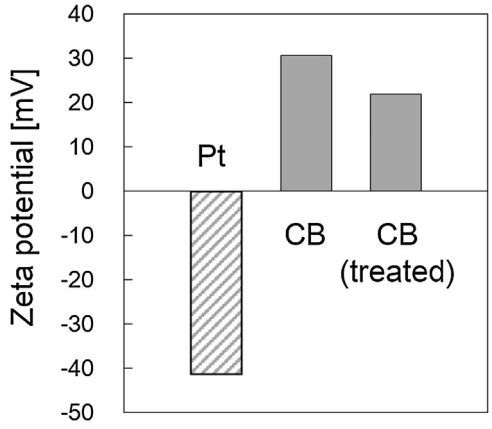

Fig. 3. Zeta potentials of agglomerated Pt nanoparticles, fresh CB, and surface-treated CB.

Fig. 3 shows the zeta potential of Pt and CB particles suspended in water. The zeta potential of Pt reached −41.2 mV, whereas those of fresh CB and surface-treated CB were about +30.6 and +22.0 mV, respectively. Because of the opposite sign of the zeta potential, we expect electrostatic interaction between Pt and CB particles in suspension. This may explain why large-scale agglomeration of Pt nanoparticles did not take place during deposition process as pointed out above. Considering the opposite sign of the zeta potential, the adsorption of Pt nanoparticles on CB is assumed to proceed in mixed suspension. If the number of nonadsorbed Pt nanoparticles becomes sufficiently small with respect to the adsorbed particles, there are not many Pt nanoparticles in suspension which cause further agglomeration during deposition process.

We performed in situ TEM observations of the agglomerated Pt nanoparticles supported on CB during heating. First, the Pt/CB samples were observed at room temperature and the observation location for heating experiment was determined. Then, we started heating the sample. Because remarkable changes in the particle morphology were observed, the heating was terminated after 60 min at 310°C. Fig. 4 shows a series of TEM images obtained during heating. At the initial state (Fig. 4(a)), we can see Pt agglomerates consisting of spherical primary particles. As the temperature increases, it becomes difficult to distinguish the shape of each primary particle because the coalescence of Pt particles progresses. To quantify this, we calculated the gyration radii of three agglomerates (p1, p2, and p3) indicated in Fig. 4(a). The variations in the particle size as well as temperature with time are shown in Fig. 5. The size of all agglomerates decreased monotonically. Presumably, the initial shape of the agglomerates formed as a result of Brownian collisions

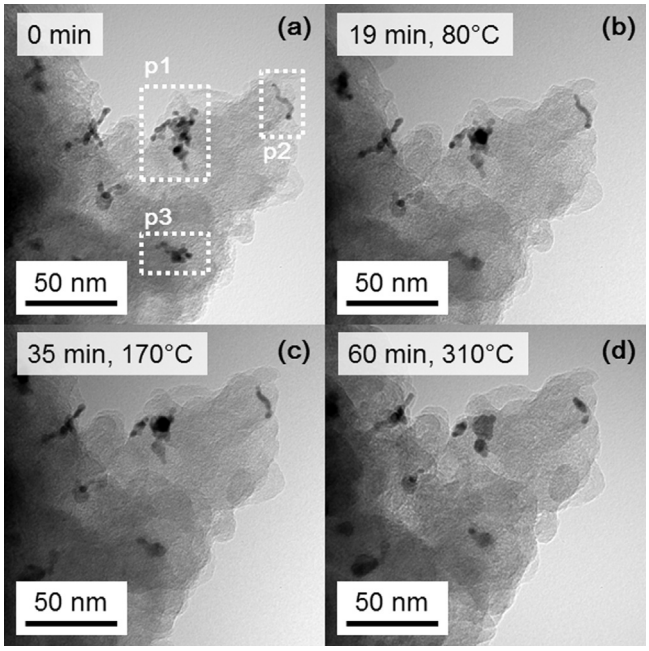

Fig. 4. Series of TEM images of agglomerated Pt nanoparticles supported on CB during heating experiment: (a) initial state at room temperature, (b) 19 min and 80°C, (c) 35 min and 170°C, and (d) 60 min and 310°C.

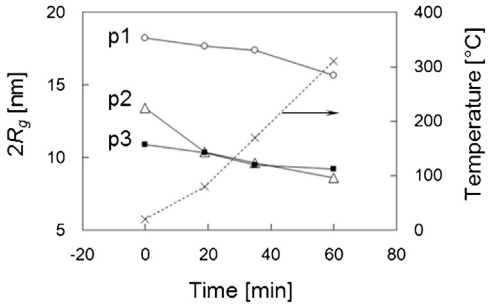

Fig. 5. Time variation of particle sizes and temperature during heating experiment.

while in suspension, and it is not always thermodynamically stable. As the temperature increased, each agglomerate acquired a more stable shape. Because of the initially unstable agglomeration morphology, the radius of gyration is useful to evaluate the degree of coalescence.

The coalescence of Pt primary particles was observed at a much lower temperature than the bulk melting point (1768°C). In addition to the size effect in the melting point decrease typically observed for nanoparticles [21,22], surface diffusion affects the progressive coalescence of Pt nanoparticles [12]. It was confirmed that the coalescence of Pt nanoparticles started below 300°C regardless of the supporting CB surface structures when they were in contact at the initial configuration. In the present in situ TEM experiment, sintering was dominated by the initially contacting particles, and it was difficult to determine the effect of the CB support. Therefore, in the next step, we used well-dispersed Pt nanoparticles to clarify the effect of the CB surface nanostructure on the stability of the supported Pt nanoparticles.

3.2. Dynamic behavior of monodispersed Pt nanoparticles

We needed to disperse well the Pt nanoparticles on the CB surface; thus, we changed the Pt preparation method to the $NaBH_4$ reduction method using Pt precursor (Fig. 1(b)). To confirm that

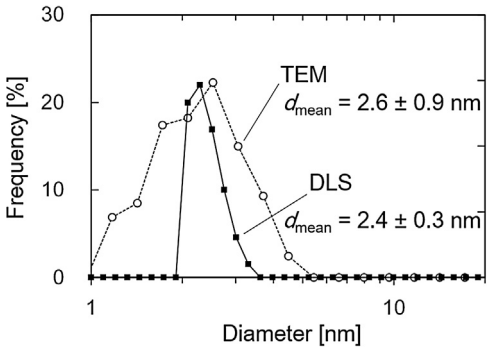

Fig. 6. Size distribution of monodispersed Pt nanoparticles measured by DLS and TEM.

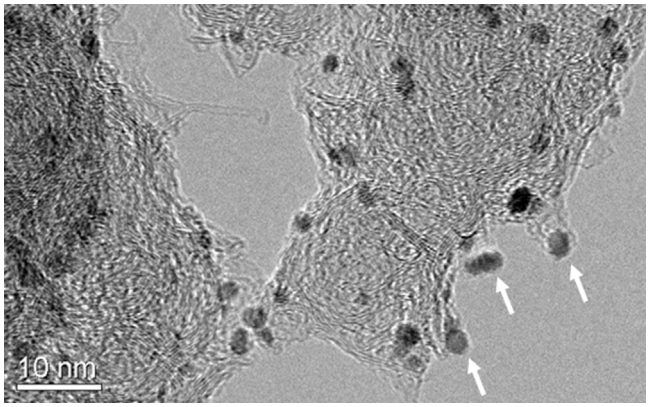

Fig. 7. TEM image of a Pt/CB sample. Protruding surface structures supporting Pt nanoparticles are indicated by the white arrows.

the monodispersed Pt nanoparticles were properly synthesized, we evaluated the size of the Pt nanoparticles in the colloidal and deposited states on CB. The results are shown in Fig. 6. In the colloidal state, the mobility diameter was measured by DLS and the mean diameter was 2.4 ± 0.3 nm. In the deposition state, the particle diameter was evaluated using the TEM images and the mean diameter was 2.6 ± 0.9 nm. Because of the uncertainty when determining the periphery of each Pt nanoparticle in TEM images, the variance was rather large compared with the DLS result. Since the mean diameters evaluated in the colloidal and deposition states agreed well, we confirmed that agglomeration of Pt nanoparticles did not take place during deposition on CB.

Fig. 7 shows a TEM image of a Pt/CB sample. The Pt nanoparticles are well dispersed on CB without agglomeration. In spite of the use of PVP which is mixed with molecular precursor of Pt, most of Pt nanoparticles synthesized in the present process are considered to be single crystals [17,23] (also see Supplementary material 1). As a result of the surface treatment of the CB sample, protruding structures were observed on the surface. It should be emphasized that Pt nanoparticles were deposited on such parts, as shown by the white arrows in Fig. 7. Considering the formation mechanism described in our previous studies [6,7], the protruding CB parts have the edges of graphitic sheet-like structure. According to Moldovan et al. who investigated the stability of Pt nanoparticles supported on graphene layers, the Pt nanoparticles were stably deposited on the edges of the few-layer graphene [9]. Therefore, we inferred that the Pt nanoparticles preferentially deposited on the protruding surface structure of CB, which apparently stably supports the Pt nanoparticles.

To investigate the thermal stability of Pt nanoparticles, we performed in situ TEM observation of Pt nanoparticles supported on surface-treated CB at high temperatures. Fig. 8 shows the temperature profile during heating. The sample was heated form room temperature to 800°C. TEM images were taken every 50°C. To minimize the influence of sample drift, we interrupted the temperature ramping when taking the images using a charge-coupled device (CCD) camera. This is the reason the temperature profile is not a straight line in Fig. 8. The averaged ramping rate was 6.3°C/min (dashed line in Fig. 8). Although the damage of a Cu grid at elevated temperatures was reported [24], we did not observe any influence of grid damage on this experiment. It appears that we could avoid the influence of grid damage on our observation because the present experimental condition was not so severe in terms of heat exposure as the case in the reference [24] and also because the grid pitch was large and the observed sample was located far from grid bars in our case.

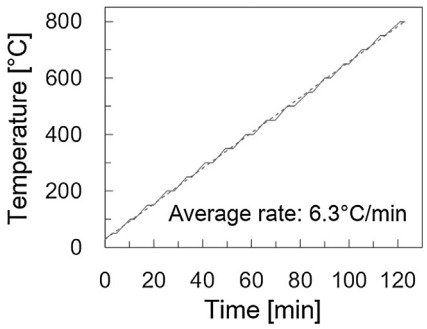

Fig. 8. Temperature profile in the heating experiment (solid line). Dashed line shows the average ramp rate over the whole heating process.

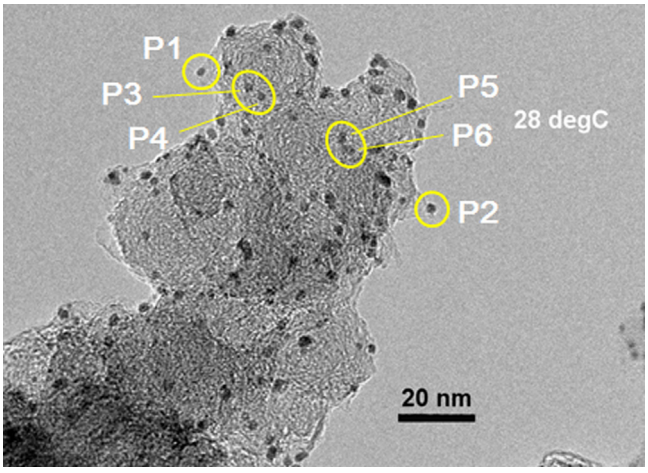

Fig. 9. TEM image of a Pt/CB sample. Pt nanoparticles used in the image analysis are identified by numbers P1–P6.

Fig. 9 shows the TEM image of the observation area in the heating experiment. The Pt nanoparticles used in the image analysis are identified by numbers P1–P6. P1 and P2 were supported on the protruding parts. Because a TEM image is two-dimensional projection of the sample, it is not possible at this stage to determine the deposition status of other particles (P3–P6) which are not located at the outer edge of CB in the TEM image. A series of magnified images for P1, P3, and P4 is shown in Fig. 10. Since we needed to manage the sample drifting by handling the microscope and adjusting the exposure time of a CCD camera, the image contrast varied in each TEM image. In addition, the sample drifting included not only the translational motion of CB support but also the rotational motion, which caused the change of observation angle on CB support from the initial condition. This makes it difficult to evaluate the exact location of Pt nanoparticle supported on CB; if the CB support showed rotational move, Pt nanoparticles stably fixed on the outer edge of CB

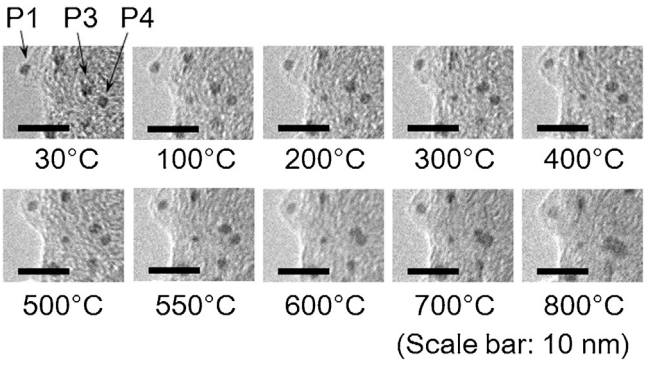

Fig. 10. Series of TEM images during the heating experiment.

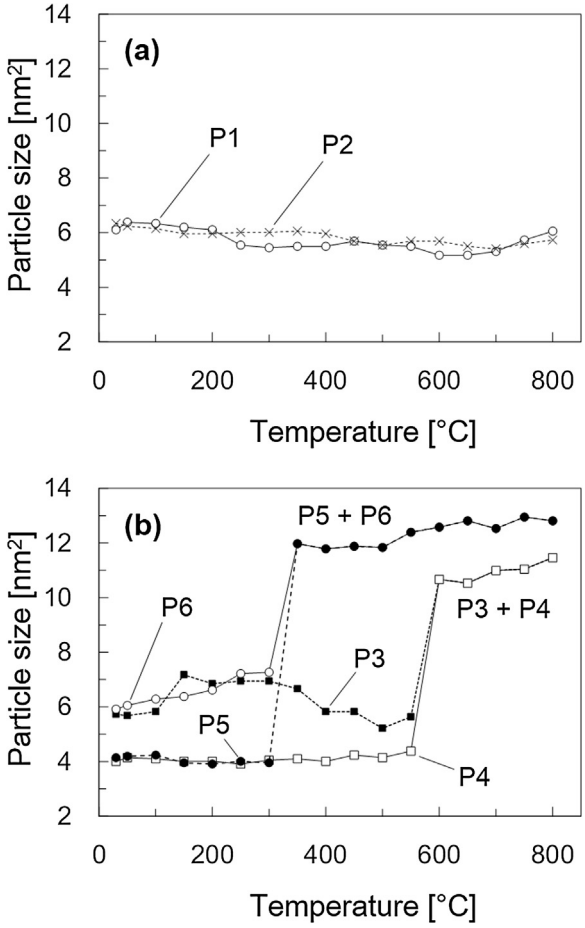

Fig. 11. Variation in size of (a) Pt nanoparticles P1 and P2 supported on protruding surface structures and (b) coalescing Pt nanoparticles P3–P6.

support would appear to migrate into the inner part of CB support in a TEM image (i.e., move in the direction perpendicular to the rotation axis). Furthermore, it should be noted that the irradiation of electron beam might damage CB support. These issues related to the dynamic behavior of sample during the heating experiment can be more easily interpreted in a movie of TEM images (Supplementary Material 2). P1 was relatively stable; it did not migrate from the protruding part and coalesce with any other particles. The distance between P3 and P4 decreased as the temperature increased, which can be seen especially at 500 and 550°C. After that, we cannot distinguish the images of P3 and P4 separately. To better show this, we evaluated the particle size by calculating the area in the TEM images. The result is shown in Fig. 11. P1 and P2, which were located on the protruding structures of CB support, did not merge with other particles and therefore the particle size did not show any remarkable change (Fig. 11(a)). On the other hand, the size of P3 and P4 discontinuously changed at 600°C (Fig. 11(b)). The same event happened for P5 and P6 at 350°C. It should be noted that the summation of particle sizes is not exactly equal to the merged size in Fig. 11(b), because the particle size evaluated by the projection area depends on particle morphology even if the particle volume is conserved. It is possible for Pt nanoparticles to coalesce at much lower temperatures than the melting point of bulk Pt once they come in contact with each other, which was experimentally demonstrated using agglomerated Pt nanoparticles (Section 3.1) and also Pt nanoparticles supported on a lacy carbon film [13]. To interpret the dynamics of particles P3 and P4, i.e., coalescing or simply overlapping in the TEM image [15], it would be helpful to examine the changes of particle morphology and image contrast. If the particles are simply overlapping in a projected image, it is highly possible that the outline of each particle's shape does not change and the image contrast at the overlapping part varies. The particles P3 and P4 (and P5 and P6 as well) appear to start changing their morphology from 600°C and not to exhibit the variation in the image contrast. On the basis of consideration here, we presume that P3 and P4 finally coalesced at around 600°C and P5 and P6 coalesced at around 350°C.

As described in Section 2.3, we used PVP as a stabilizer to obtain monodispersed Pt nanoparticles. Excellent dispersion of Pt/CB in water was achieved with the help of PVP attached on the surface of Pt particles and probably CB as well. Hence, we expect that PVP was attached on the Pt/CB sample used in the heating TEM experiment. Because PVP thermally decomposes at around 350°C [25,26], we inferred that the dispersing effect of PVP was lost at the temperature where P5 and P6 coalesced. P1 and P2 were located at their initial positions even after passing the decomposition temperature of PVP. Thus, it appears that the thermal decomposition of PVP does not affect the stability of Pt nanoparticles deposited on stable positions of the CB surface. Since the number of particles observed in the present experiment is limited, the further investigation is desirable to validate the point suggested here through experiments with a large number of Pt nanoparticles.

To further examine the stability of Pt nanoparticles on the treated surface of CB, we observed the Pt nanoparticles deposited on the amorphous carbon film on the TEM grid used in the heating experiment reported above. It would be straightforward to perform a heating experiment using a pristine CB sample at the same condition in order to examine the positive effect of CB surface nanostructure on Pt supporting. However, it is technically difficult to exactly repeat the temperature profile which is determined when managing sample drifting in each heating experiment. Consequently, we evaluated the Pt nanoparticles supported on the carbon film that were exposed to the identical temperature history shown in Fig. 8. It should be noted that it is necessary to perform experiments with a sufficiently large number of particles for concluding the positive effect of CB surface treatment because the number of particles observed in in-situ TEM experiment is limited. Considering the synthesis process (Fig. 1(b)), we can assume that the Pt nanoparticles supported on the carbon film had approximately the same number density on the film surface as the Pt nanoparticles supported on CB. Before starting the heating experiment, we took the images of Pt nanoparticles supported by the carbon film as well as Pt/CB particles. After completing the heating experiment, we observed again the large area in the TEM grid. Although we did not fix the observation area of the Pt nanoparticles deposited on the carbon film, we took representative images of the sample. Using these TEM images, we compared the size of the Pt nanoparticles before and after the heating experiment. We counted nearly 250 Pt nanoparticles in this analysis; we consider the number of par-

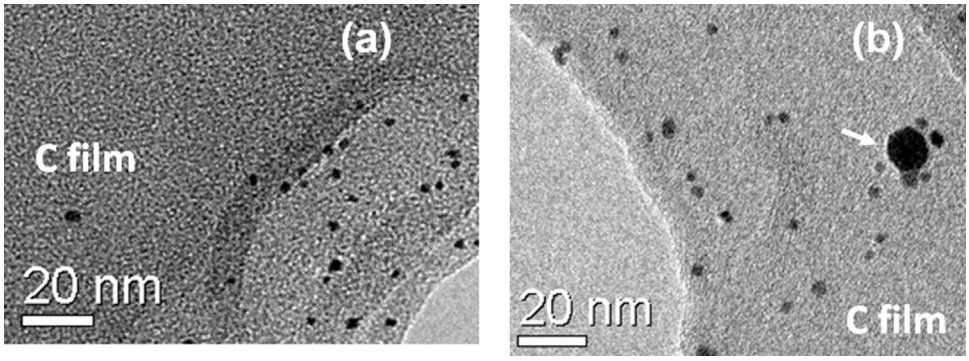

Fig. 12. TEM image of Pt nanoparticles supported on an amorphous carbon film: (a) before and (b) after the heating experiment.

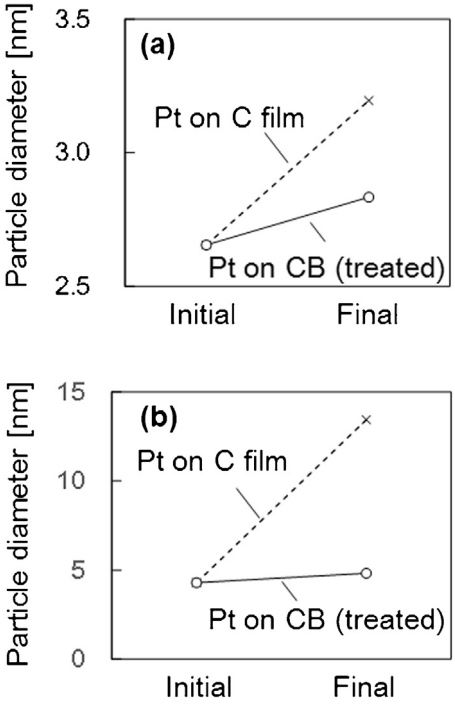

Fig. 13. Change in size of Pt nanoparticles supported on an amorphous carbon film and surface-treated CB. (a) Mean diameter. (b) Maximum diameter.

ticles is sufficient to evaluate the mean diameter according to our previous work [27]. Fig. 12(a) shows a TEM image taken before the heating experiment. The Pt nanoparticles are well dispersed on the film, as observed on the CB surface (Figs. 7 and 9). Fig. 12(b) shows a TEM image of the sample after heating up to 800°C (Fig. 8). We found large Pt nanoparticles whose size was not observed before heating (indicated by the white arrow), even though there were some Pt nanoparticles that did not show any remarkable change in size. Fig. 13(a) and (b) shows the change in the mean diameter and maximum diameter, respectively. For Pt/CB samples, we did not find such large Pt nanoparticles as the one shown in Fig. 12(b). To emphasize this difference, we show the maximum diameter of Pt nanoparticles in Fig. 13(b). For Pt nanoparticles supported on the surface-treated CB, both mean and maximum diameters show small increases after heating. On the other hand, for Pt nanoparticles supported on carbon film, the mean diameter increased more than that of Pt on CB and the difference is remarkable for the maximum particle diameter. The Pt nanoparticles supported by a carbon film were not exposed to the electron beam during the heating experiment. Asoro et al. stated that the electron beam did not seem to have a significant effect on the sintering of Pt nanoparticles [13]. Therefore, we infer that the observed difference in the Pt growth originated from the different surface characteristics of supporting carbon materials. The discussion here is based on the TEM observations that are limited by the small number of Pt nanoparticles compared with the number in a real-scale catalyst system. Nevertheless, this approach showed one aspect of the characteristics regarding the stability of Pt nanoparticles and its dependence on the nanoscale surface structure of the support carbon material.

4. Conclusions

We investigated the thermal stability of Pt nanoparticles supported on CB with nanoscale protruding surface structures. We have confirmed that the coalescence of Pt nanoparticles progresses below 300°C regardless of the supporting CB surface structures when they are in contact. The $NaBH_4$ reduction method is useful to synthesize well-dispersed Pt nanoparticles, and Pt nanoparticles can deposit on the protruding parts of the CB surface. In situ TEM observations of Pt nanoparticles during heating showed the differences in the Pt nanoparticle stability depending on the deposition locations of the CB surface. When using a stabilizer such as PVP, it might be possible to remove the stabilizer by heat exposure without damaging the catalyst nanoparticles. On the basis of discussion here, the possibility of surface-treated CB as a stable catalyst support is suggested. In future, it is expected to examine the application of Pt catalysts supported on surface-treated CB to electrochemical reactions and investigate the performance improvement owing to the surface nanostructure.

Acknowledgments

This work was supported by JSPS KAKENHI Grant Number 26889056 (Grant-in-Aid for Research Activity Start-up). A part of this work was supported by “Nanotechnology Platform” (project No. 12024046) of the Ministry of Education, Culture, Sports, Science and Technology (MEXT), Japan. The authors thank Professor Kanjiro Torigoe at Tokyo University of Science for his support in preparing Pt nanoparticles.

Appendix A. Supplementary data

Supplementary data associated with this article can be found, in the online version, at http://dx.doi.org/10.1016/j.apcatb.2016.02.049.

References

[1] S. Shahgaldi, J. Hamelin, Improved carbon nanostructures as a novel catalyst support in the cathode side of PEMFC: a critical review, Carbon 94 (2015) 705–728.

[2] M. Hara, M. Lee, C.H. Liu, B.H. Chen, Y. Yamashita, M. Uchida, H. Uchida, M. Watanabe, Electrochemical and Raman spectroscopic evaluation of Pt/graphitized carbon black catalyst durability for the start/stop operating condition of polymer electrolyte fuel cells, Electrochim. Acta 70 (2012) 171–181.
[3] H. Kim, A.W. Robertson, S.O. Kim, J.M. Kim, J.H. Warner, Resilient high catalytic performance of platinum nanocatalysts with porous graphene envelope, ACS Nano 9 (2015) 5947–5957.
[4] J.B. Donnet, C. Bansal, M.J. Wang, Carbon Black, 2nd ed., Marcel Dekker, New York, 1993.
[5] Y. Kameya, K. Hanamura, Kinetic and Raman spectroscopic study on catalytic characteristics of carbon blacks in methane decomposition, Chem. Eng. J. 173 (2011) 627–635.
[6] Y. Kameya, K. Hanamura, Carbon black texture evolution during catalytic methane decomposition, Carbon 50 (2012) 3503–3512.
[7] Y. Kameya, K. Hanamura, Variation in catalytic activity of carbon black during methane decomposition: active site estimations from surface structural characteristics, Catal. Lett. 142 (2012) 460–463.
[8] Y. Kameya, T. Hayashi, M. Motosuke, Oxidation-resistant graphitic surface nanostructure of carbon black developed by ethanol thermal decomposition, Diam. Relat. Mater. 65 (2016) 26–31.
[9] M.S. Moldovan, H. Bulou, Y.J. Dappe, I. Janowska, D. Bégin, C. Pham-Huu, O. Ersen, On the evolution of Pt nanoparticles on few-layer graphene supports in the high-temperature range, J. Phys. Chem. C 116 (2012) 9274–9282.
[10] X. Li, I.M. Hsing, The effect of the Pt deposition method and the support on Pt dispersion on carbon nanotubes, Electrochim. Acta 51 (2006) 5250–5258.
[11] L.C. Gontard, R.E. Dunin-Borkowsky, D. Ozkaya, Three-dimensional shapes and spatial distributions of Pt and PtCr catalyst nanoparticles on carbon black, J. Microscopy 232 (2008) 248–259.
[12] S.B. Simonsen, I. Chorkendorff, S. Dahl, M. Skoglundh, J. Sehested, S. Helveg, Direct observations of oxygen-induced platinum nanoparticle ripening studied by in situ TEM, J. Am. Chem. Soc. 132 (2010) 7968–7975.
[13] M.A. Asoro, D. Kovar, Y. Shao-Horn, L.F. Allard, P.J. Ferreira, Coalescence and sintering of Pt nanoparticles: in situ observation by aberration-corrected HAADF STEM, Nanotechnology 21 (2010) 025701.
[14] F. Hasché, M. Oezaslan, P. Strasser, In situ observation of the thermally induced growth of platinum-nanoparticle catalysts using high-temperature X-ray diffraction, Chem. Phys. Chem. 13 (2012) 828–834.
[15] M.A. Asoro, P.J. Ferreira, D. Kovar, In situ transmission electron microscopy and scanning transmission electron microscopy studies of sintering of Ag and Pt nanoparticles, Acta Mater. 81 (2014) 173–183.
[16] D. Gardini, J.M. Christensen, C.D. Damsgaard, A.D. Jensen, J.B. Wagner, Visualizing the mobility of silver during catalytic soot oxidation, Appl. Catal. B 183 (2016) 28–36.
[17] K. Torigoe, Y. Nakajima, K. Esumi, Preparation and characterization of colloidal silver-platinum alloys, J. Phys. Chem. 97 (1993) 8304–8309.
[18] C.A. Schneider, W.S. Rasband, K.W. Eliceiri, NIH image to ImgeJ: 25 years of image analysis, Nat. Methods 9 (2012) 671–675.
[19] A.M. Brasil, T.L. Farias, M.G. Carvalho, A recipe for image characterization of fractal-like aggregates, J. Aerosol Sci. 30 (1999) 1379–1389.
[20] M.L. Eggersdorfer, S.E. Pratsinis, The structure of agglomerates consisting of polydisperse particles, Aerosol Sci. Technol. 46 (2012) 347–353.
[21] H. Sakai, Surface-induced melting of small particles, Surf. Sci. 351 (1996) 285–291.
[22] E. Kim, B. Lee, Size dependency of melting point of crystalline nano particles and nano wires: a thermodynamic modeling, Metals Mater. Int. 15 (2009) 531–537.
[23] Y. Jiang, Y. Wang, Y.Y. Zhang, W. Yuan, C. Sun, X. Wei, C.N. Brodsky, C.K. Tsung, J. Li, X. Zhang, S.X. Mao, S. Zhang, Z. Zhang, Direct observation of Pt nanocrystal coalescence induced by electron-excitation-enhanced van der walls interactions, Nano Res. 7 (2014) 308–314.
[24] Z. Zhang, D. Su, Behaviour of TEM metal grids during in-situ heating experiments, Ultramicroscopy 109 (2009) 766–774.
[25] Y.K. Du, P. Yang, Z.G. Mou, N.P. Hua, L. Jiang, Thermal decomposition behaviors of PVP coated on platinum nanoparticles, J. Appl. Polym. Sci. 99 (2006) 23–26.
[26] N.V. Long, M. Ohtaki, M. Nogami, T.D. Hien, Effects of heat treatment and poly(vinylpyrrolidone) (PVP) polymer on electrocatalytic activity of polyhedral Pt nanoparticles towards their methanol oxidation, Colloid Polym. Sci. 289 (2011) 1373–1386.
[27] Y. Kameya, K.O. Lee, Ultra-small-angle X-ray scattering characterization of diesel/gasoline soot: sizes and particle-packing condition, J. Nanopart. Res. 15 (2013) 2006.